Desalination and Water Treatment
www.deswater.com

doi: 10.5004/dwt.2017.21267

85 (2017) 25–35
August

Study on the preparation and properties of Cu(II) molecularly imprinted membrane (Cu(II)/MIM/PVDF)

Xiaojiao Yu[a,*], Song Kou[a], Qian Yang[a], Yingjuan Zhao[a], Yuchen Wei[b], Binghua Yao[a]

[a]*School of Science, Xi'an University of Technology, No. 5 South Jinhua Road, Xi'an 710048, China, Tel./Fax: +86 29 82066360; emails: yxjw@xaut.edu.cn (X. Yu), 442505576@qq.com (S. Kou), 914730841@qq.com (Q. Yang), 53091525@qq.com (Y. Zhao), bhyao@xaut.edu.cn (B. Yao)*

[b]*School of Science, The Hong Kong University of Science and Technology, Clear Water Bay, Kowloon, Hong Kong, China, Tel. +00852 53449506; email: wych82313102@gmail.com (Y. Wei)*

Received 7 January 2017; Accepted 30 July 2017

ABSTRACT

A Cu(II) molecularly imprinted modified membrane is prepared by graft polymerization of α-methacrylic acid on the surface of a polyvinylidene fluoride (PVDF) membrane. The modified membrane is characterized using scanning electron microscope, X-ray diffraction, attenuated total reflection–Fourier-transform infrared spectrometer, X-ray photoelectron spectrophotometer, contact angle, thermogravimetric analysis–differential thermal analysis and an electronic tensile testing machine. Permeability and selectivity of the modified membrane are also evaluated via pure water flux and transfer experiments. The results indicate that the microvoids of the modified membrane surface are uniformly distributed and change obviously, the amorphous state area of modified membrane increases, and the original crystal characteristics of the PVDF membrane are maintained. The α-methacrylic acid grafts onto PVDF membrane surface and the molecularly imprinted polymer layer are combined with PVDF through C–O bond. The hydrophobicity of modified membrane decreases and the surface energy increases. The mechanical properties of the membrane become weak after modification. The permeability coefficient of the modified membrane is higher than that of a PVDF membrane. The transfer rate of Cu(II) can reach 92% through the Cu(II) molecularly imprinted modified membrane, whereas the transfer rate of Mn(II), Co(II) and Ni(II) is less than 10%. The modified membrane shows excellent selectivity and permeability for Cu(II).

Keywords: Polyvinylidene fluoride membrane; Surface modification; Molecularly imprinted modified membrane; Performance

1. Introduction

As wastewater containing heavy metal ions that produce a variety of conditions detrimental to daily human life has become increasingly widespread globally, human health has suffered, and this seriousness of the situation has gradually attracted significant public attention [1,2]. Many researchers have concentrated their efforts on the development of innovative approaches to improve conventional water treatment methods so this issue can be thoroughly resolved [3–5]. Among various new methods, membrane separation attracted considerable attention owing its outstanding advantages of high structural stability, high mass-transfer flux, low energy consumption and non-secondary pollution [6–9]. Using a polyvinylidene fluoride (PVDF) membrane as the support layer shows more excellent characteristics, such as better thermal stability, chemical stability and hydrophobicity than those of other membrane materials [10–13]. As a result, it has been commonly used in ultrafiltration, microfiltration, and material separation process [14–19]. However, there are still some deficiencies in the use of PVDF membranes for metal ions separation, such as selectivity of metal ions, solvent stability, hydrophilic, and antifouling ability.

* Corresponding author.

Therefore, the structure and properties of PVDF membrane must be improved via surface modification. The numerous methods of modifying PVDF membranes include surface coating, photografting, surface-initiated atom transfer radical polymerization, and graft polymerization [20–23]. Surface modification not only maintains the good physical properties of PVDF membranes but also endows the surface with new properties. Molecularly imprinting technology is a method in which a monomer provides binding sites to combine with the template molecule to form a highly cross-linked polymeric layer, on which microvoids tally with the shape of the template molecule after elution. It is widely believed that molecularly imprinted structures possess high selectivity for template molecules, and thus it is suitable for separating and recycling metal ions in wastewater [24–28]. This structure also possesses other advantages, including easy preparation and high chemical stability under various experimental conditions of pH, temperature, and solvents [29–31]. Furthermore, compared with liquid membranes, molecularly imprinted membranes (MIMs) based on PVDF can ensure minimal membrane solvent loss through vaporization and dissolution, and they barely cause recontamination by the membrane solvent. Meanwhile, if chemical bonds exist between the PVDF membrane and MIM layer, the structure stability of modified membrane will be enhanced so as to promote the significant reutilization of the membrane for practical application. Owing to these merits, MIM/PVDF shows promising potential in various fields, especially in water treatment. To the best of our knowledge, although PVDF and MIM have been extensively studied separately, little has been reported, to date, on the preparation of a supported liquid membrane combined with molecular imprinting technology.

The objective of this paper is to investigate the preparation and properties of Cu(II) MIM on a PVDF (Cu(II)/MIM/PVDF) membrane under UV light irradiation using Cu(II) as a template, α-methacrylic acid (MAA) as a functional monomer, and ethylene glycol dimethacrylate (EDMA) as a cross-linking agent. The surface morphology and properties of the modified membrane are analyzed using various instruments and experiments, and the result shows a significant improvement in the membrane performance of Cu(II)/MIM/PVDF.

2. Experiment

2.1. Materials

PVDF microporous membranes in matrix form were purchased from Shanghai Diqing Filtering Technology Co., Ltd. (China). MAA, the functional monomer, was obtained from Tianjin Tianda Chemical Co., Ltd. (China). EDMA, the cross-linking agent, was purchased from Beijing Eastern Acrylic Chemical Technology Co., Ltd. (China). 2,2′-azobisisobutyronitrile (AIBN) was supplied by Shanghai Shanpu Chemical Co., Ltd. (China) and benzophenone (BP) was purchased from Nantong Huikang International Enterprise Co., Ltd. (China). The membrane performance experimental setup and UV light device were both self-made.

2.2. Synthesis of molecularly imprinted modified membrane

The PVDF microporous membrane was placed in sulfuric acid (3.0 mol L^{-1}) for 1 h and then washed with deionized water. $CuSO_4 \cdot 5H_2O$ (0.9500 g) was dissolved in 5 mL of deionized water to form solution (1), while 1.94 mL of MAA was dissolved in 5 mL of methyl cyanide to form solution (2). After mixing solutions (1) and (2) with 1 mL of Span-80 to ensure the molar ratio of the template molecule to monomer was 1:4, the suspension was stirred for 10 min to form solution (3). AIBN (0.0370 g) and EDMA (20 mL) were added to solution (3) and then ultrasonic oscillation performed for 20 min to obtain solution (4). The PVDF membrane with pretreatment was immersed into BP (0.6%) solution for 45 min, and then immersed into solution (4) for 90 min. Subsequently, the membrane was exposed to UV light (λ = 365 nm) for 4 h to complete the polymerization; the polymerization process equation is shown in Fig. 1. After polymerization, the membrane was washed with ethanol–sodium hydroxide solution several times to remove the residue until there was none of the template molecule in the wastewater of the samples, and then it was dried at room temperature. Cu(II)/MIM/PVDF with molar ratios of the template molecule and monomer of 1:5 and 1:6 was prepared in accordance with the above procedures.

The graft yield (GY) of the modified PVDF membrane was calculated by the weighing method according to Eq. (1) [32]:

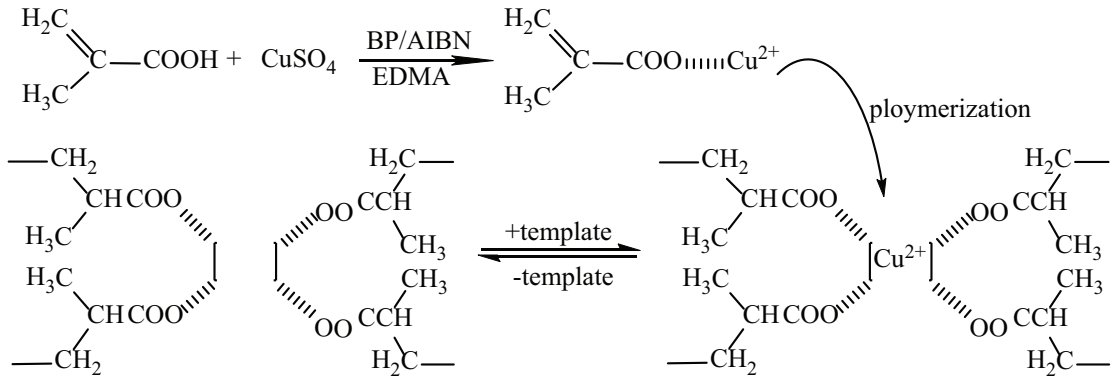

Fig. 1. Polymerization process equation.

$$\mathrm{GY}(\%) = \frac{m_1 - m_0}{m_0} \times 100 \quad (1)$$

where m_1 and m_0 are the weights of modified PVDF membrane and original PVDF membrane, respectively.

2.3. Morphology and properties measurement of Cu(II)/MIM/PVDF

The surface morphology of the PVDF membrane and Cu(II)/MIM/PVDF were observed using a field emission scanning electron microscope (SEM, Model JSM-6700F JEOL Corp., Japan). All membrane samples were coated with a thin layer of gold before testing. The X-ray diffraction (XRD) patterns of the PVDF membrane and Cu(II)/MIM/PVDF were measured on an X-ray diffractometer (6100 type, Shimadzu Corp., Japan) using Cu Kα radiation, a fixed power source at 40 kV and 40 mA, and a scanning speed of 4° min^{-1}. ATR–FTIR spectroscopic analysis of the top surface of the membrane was made using an attenuated total reflection–Fourier-transform infrared spectrometer (ATR–FTIR, IRAffinity-1 type, Shimadzu Corp., Japan) in the range of 650–4,000 cm^{-1}. An X-ray photoelectron spectrophotometer (XPS, K-Alpha type, Thermo Fisher Scientific, USA) was used to analyze the element content and chemical bonds of the membrane surface before and after performing the molecular imprinting operation. To avoid the influence of pollution on the membrane surface, all the membrane samples were etched for 5 s before analysis. The contact angle and surface energy of the membrane were measured using a contact angle measuring instrument (CA, Model OCA20, Dataphysics, Germany). The pendant drop method was used to let a droplet (2 μL) fall on the membrane surface to determine the contact angle and surface energy of the membrane. The contact time of each sample was 5 s and each sample was measured three times, with the average value taken to minimize the experimental error. Thermogravimetric analysis (TGA) and differential thermal analysis (DTA) were performed with a thermogravimetric analyzer (TGA–DTA, DTG-60AH type, Shimadzu Corp., Japan) to estimate the membrane thermal stability at a temperature interval varying from 20°C to 1,000°C with a heating rate of 20°C min^{-1}. The mechanical properties of the membrane were measured using an LCD electronic tensile testing machine (EMT 2503 type, Shenzhen Sans Testing Machine Co., Ltd., China) at 20°C. Samples were cut to 10 cm in length and 1 cm in width from the membrane sheet. The thickness of the membrane was measured using a thickness tester at 10 different positions before measurement. The initial length between two clamps was 3 cm and the elongation velocity was 20 mm min^{-1}.

2.4. Pure water fluxes and rejection measurement of Cu(II)/MIM/PVDF

To evaluate the permeability of membranes, a self-made dynamic circulation flat plate type membrane performance experimental setup was used to study pure water fluxes of the membrane; a schematic of the setup is shown in Fig. 2. The PVDF membrane or Cu(II)/MIM/PVDF was washed with ethanol and deionized water in turn, followed by natural drying in air. The membrane was then installed on the experimental

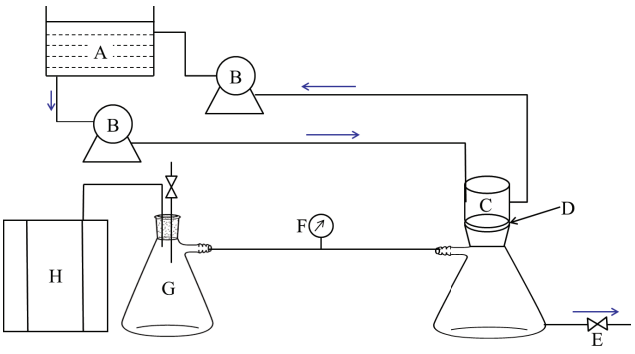

Fig. 2. The schematic of membrane performance experimental setup: (A) feed tank, (B) peristaltic pump, (C) test cell, (D) membrane, (E) valve, (F) pressure gauge, (G) safety bottle, and (H) vacuum pump.

setup. The effective membrane area was 1.32 × 10^{-3} m^2. The membrane was initially hydraulically compacted by applying a pressure of 0.05 MPa for 30 min, followed by pure water flux measurement during a stable state. The applied pressure was subsequently reduced to 0.01 MPa. The effluent liquid volume was determined for 2 h with an interval of 5 min. Pure water flux was calculated using Eq. (2) [33]:

$$J_{\mathrm{W}} = \frac{V}{A\Delta t} \quad (2)$$

where J_w is the pure water flux (L·m^{-2}·h^{-1}), V the permeate volume (L), A the membrane effective surface area (m^2) and Δt the time taken to collect the permeate (h).

The rejection rate was tested using the experimental setup shown in Fig. 2. The rejection (R) is calculated as Eq. (3):

$$R(\%) = \frac{C_{\mathrm{feed}} - C_{\mathrm{perm}}}{C_{\mathrm{feed}}} \times 100 \quad (3)$$

where C_{feed} and C_{perm} are the Cu(II), Mn(II), Co(II), and Ni(II) concentrations (mol L^{-1}) of the feed solution and permeate solution, respectively. The rejection rate was tested in accordance with the above procedures for the pure water flux measurement. In the rejection experiments, the initial concentration of Cu(II), Mn(II), Co(II), and Ni(II) was 4 × 10^{-4} mol L^{-1}, and the metal ion concentration was determined for 5 h with an interval of 20 min.

2.5. Selectivity measurements for Cu(II)/MIM/PVDF

Cu(II)/MIM/PVDF was immersed in kerosene with 2-ethylhexyl-2-ethylhexyl phosphonate (P507, 7.0%) for 1 h before the transfer experiments, and then the membrane was dried and fixed on the transfer instrument. The schematic of the equipment used for the selectivity measurements is shown in Fig. 3. The feed solution and stripping solution of plasma intensity were added to the feed solution bath and stripping solution bath, respectively. The feed solution consists of a 0.5 mol L^{-1} HAc–NaAc solution with 5 × 10^{-4} mol L^{-1} of Cu(II), Ni(II), Co(II), and Mn(II) added to it. A 1.0 mol L^{-1} H_2SO_4

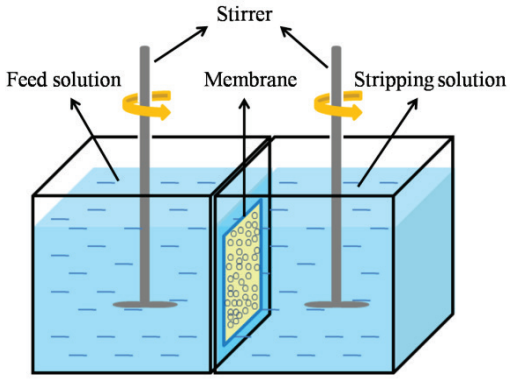

Fig. 3. The schematic diagram of membrane selectivity measurement experimental set up.

solution was used as a stripping solution. All the transfer processes were carried out at room temperature and a 0.5 mL sample from the feed solution and stripping solution was sampled every 10 min. The metal ions were measured by atomic absorption spectrometry (AA-6300C type, Shimadzu Corp., Japan). The experimental process for selectivity measurements of the PVDF membrane was carried out in accordance with the above procedures.

2.6. Determination of permeability coefficient for Cu(II)/MIM/PVDF

The permeability of MIM/PVDF for Cu(II) is expressed by permeability coefficient (P_c), which can be calculated by the following Eq. (4):

$$-\ln\frac{c_t}{c_0}=\frac{P_c A\varepsilon}{V_f}t \tag{4}$$

where c_t is the concentration of Cu(II) at t, c_0 the initial concentration of Cu(II), P_c permeability coefficient, A the effective area of membrane (cm^2), V_f the volume of feed solution, and ε the porosity of membranes.

The porosity of the membranes can be estimated by Eq. (5) [34]:

$$\varepsilon(\%)=\left(\frac{m_w-m_d}{\rho_w A\delta}\right)\times 100 \tag{5}$$

where m_w indicates the wet sample mass (g), m_d the dry sample mass (g), ρ_w the density of pure water (g cm^{-3}), and δ the thickness of membrane (cm).

3. Results and discussion

3.1. SEM analysis

The surface morphology of the PVDF membrane and Cu(II)/MIM/PVDF with different ratios of the template molecule to the monomer of 1:4, 1:5 and 1:6 are shown in Fig. 4. Figs. 4(a), (d), (g), and (j) show that there is an obvious polymeric layer on the surface of Cu(II)/MIM/PVDF compared with the PVDF membrane, and the microvoids are distributed more evenly. The pore size distribution of membrane surface is more uniform when the ratio of the template molecule to the monomer is 1:5. This indicates that a good MIM has been prepared. It can be found, by comparison of Figs. 4(b), (e), (h), and (k), that there has been a decrease in the micropore diameter of Cu(II)/MIM/PVDF to about 1–3 μm, indicating a better selectivity of Cu(II)/MIM/PVDF for the template molecule. It can be seen from Figs. 4(c), (f), (i), and (l) that the modified membrane retains the finger hole structure of the pure PVDF membrane; moreover, the spongy structure of the modified membrane bottom layer is looser than that of the pure PVDF membrane, the benefit of which is to reduce the permeation resistance and improve the permeability of the modified membrane.

3.2. XRD analysis

The XRD patterns of the PVDF membrane and Cu(II)/MIM/PVDF are shown in Fig. 5. In the figure, curves (b), (c), (d), and (e) represent the patterns of Cu(II)/MIM/PVDF with different ratios of the template molecule to the monomer of 1:4, 1:5, 1:5, and 1:6, respectively. The light triggering times were 4, 4, 6, and 4 h, respectively. It can also be seen from Fig. 5 that the pure PVDF membrane shows three peaks at 2θ values of 18.54°, 19.89°, and 39.4°; these are typical α-phase PVDF characteristics of diffraction peaks that correspond to (020), (110), and (131) planes of the crystalline region, respectively [35]. It can further be seen from curves (b), (c), and (e) of the figure that when the ratios of the template molecule to the monomer are 1:4, 1:5, and 1:6, respectively, there are no obvious changes in the characteristic peak of Cu(II)/MIM/PVDF. With the light triggering time extension, the Cu(II)/MIM/PVDF characteristic peak intensity was weakened. When the light triggering time was 6 h, the α-phase characteristic peak at 39.4° disappeared. This may be due to the strong polarity of the C–F bond rupture, and then a reaction with the cross-linking agent to form new chemical bonds. The original crystal type of PVDF was destroyed, thereby reducing the PVDF crystallinity. The crystal structure changed from order to disorder, and the amorphous regions of membrane increased to a certain extent. When the light triggering time was 4 h, there was no obvious change in the characteristic peak of PVDF, indicating that Cu(II)/MIM/PVDF retains the good crystalline state of the PVDF membrane's crystal form.

3.3. ATR–FTIR analysis

The ATR–FTIR spectra of the PVDF membrane and Cu(II)/MIM/PVDF are displayed in Fig. 6. In the figure, the typical characteristic peaks of PVDF at 1401.15, 1234.08, 1172.41, 1069.09, 876.83, and 833.14 cm^{-1} are found for Cu(II)/MIM/PVDF [36]. Compared with Fig. 6(a), the characteristic absorption peak intensity of the PVDF membrane was reduced with an increase of the ratio of the template molecule and the monomer in Figs. 6(b)–(d), and no obvious change in the characteristic absorption spectrum of the carbon chain skeleton was observed. This indicates that the C–F or C–H bonds of Cu(II)/MIM/PVDF were broken to a certain extent, and that the PVDF membrane skeleton structure was not damaged. It can be seen from Figs. 6(b)–(d) that the new characteristic bands are observed at 1724.99 and 3022.45 cm^{-1}

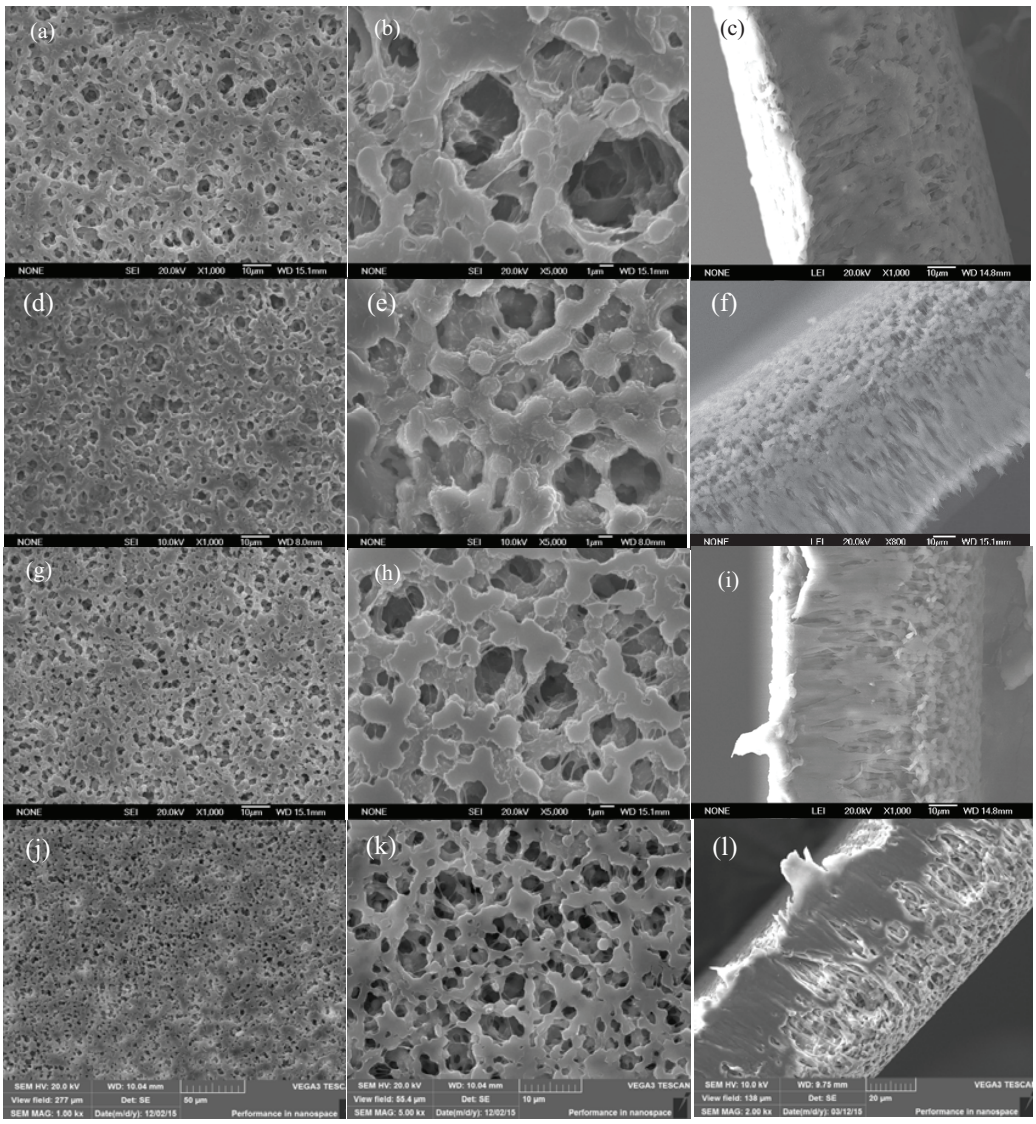

Fig. 4. SEM images of (a, b and c) PVDF membrane, (d, e and f) Cu(II)/MIM/PVDF(1:6), (g, h, and i) Cu(II)/MIM/PVDF(1:5), (j, k, and l) Cu(II)/MIM/PVDF (1:4).

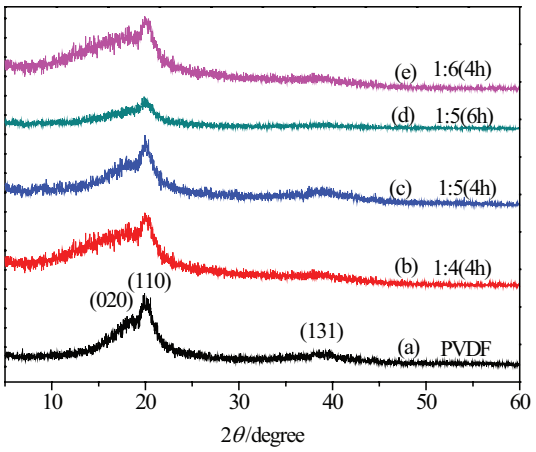

Fig. 5. The XRD patterns of (a) PVDF membrane and (b, c, d, and e) Cu(II)/MIM/PVDF.

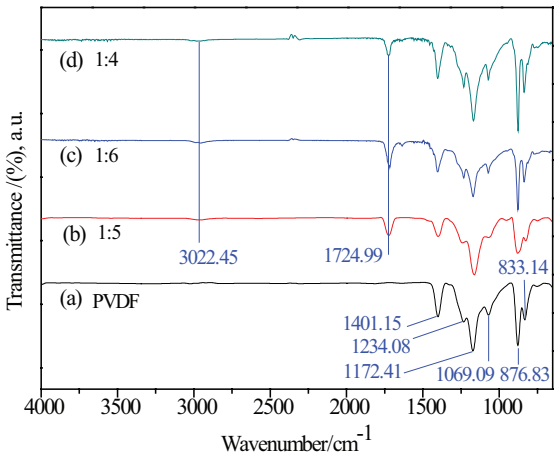

Fig. 6. ATR–FTIR spectra of (a) PVDF and (b, c, and d) Cu(II)/MIM/PVDF.

and that they belong to carbonyl and methyl groups. The presence of these bands confirms the deposition of a new imprinted layer on the PVDF membrane surface. Further insights were drawn from the XPS investigations. When the ratios of template molecule to the monomer were 1:4, 1:5, and 1:6, the GYs of the modified PVDF membrane were 21.3%, 22.8%, and 23.8%, respectively, which indicate that GY does not significantly change within the scope of the ratio of the template molecule to the monomer.

3.4. XPS analysis

Fig. 7 shows the XPS spectra of the PVDF membrane and Cu(II)/MIM/PVDF. In Fig. 7(a), curve (1) represents the spectra of the PVDF membrane, while curve (2) represents the spectra of Cu(II)/MIM/PVDF. In curve (1), there are two peaks located at 287.0 eV for C 1s binding energy and at 688.6 eV for F 1s binding energy, respectively. Simultaneously, the Auger peaks of F are located at 860.08 and 834.0 eV, while the Auger peak of C is located at 1228.0 eV, thus proving further verification for the presence of C 1s and F 1s binding energies. In comparison, curve (2) shows not only the presence of C 1s and F 1s, but also two new peaks at 532.0 and 1072.1 eV for the feature peak and Auger peak of O 1s. This condition can be explained as the combination between PVDF and MIM layers in the form of a chemical bond that introduces the elemental O of MAA and EDMA. In Fig. 7(b), two C 1s peaks are located at 291.0 and 286.4 eV, corresponding to C–F_2 and C–H_2 binding energies, respectively. The areas of the two peaks are calculated as 1.893914 and 2.027313, respectively, in accordance with the molecular structure of PVDF. It can be found from the comparison of Figs. 7(c) and (d) that there is a new rise at the bottom of the C–H feature peak, and, at the same time, that the C–F feature peak is obviously decreased, indicating that there is a break in the C–F bond in PVDF and recombination with other groups. Fig. 7(d) shows the results of fitted peaks with a new C 1s peak located at 289.3 eV for –O–C=O binding energy. To avoid the influence of residual such as MAA and EDMA on the surface or in the microvoids, etching and elution were performed before analysis. Therefore, it can be inferred that the –O–C=O group in the MIM layer substitutes element F in C–F to combine PVDF with the MIM layer after polymerization in the form of a chemical bond rather than deposition, which indicates that α-methacrylic acid was successfully grafted to the surface of PVDF.

3.5. Thermostability analysis

The DTA–TGA data of the PVDF membrane and Cu(II)/MIM/PVDF are shown in Fig. 8. Fig. 8(a) shows that the

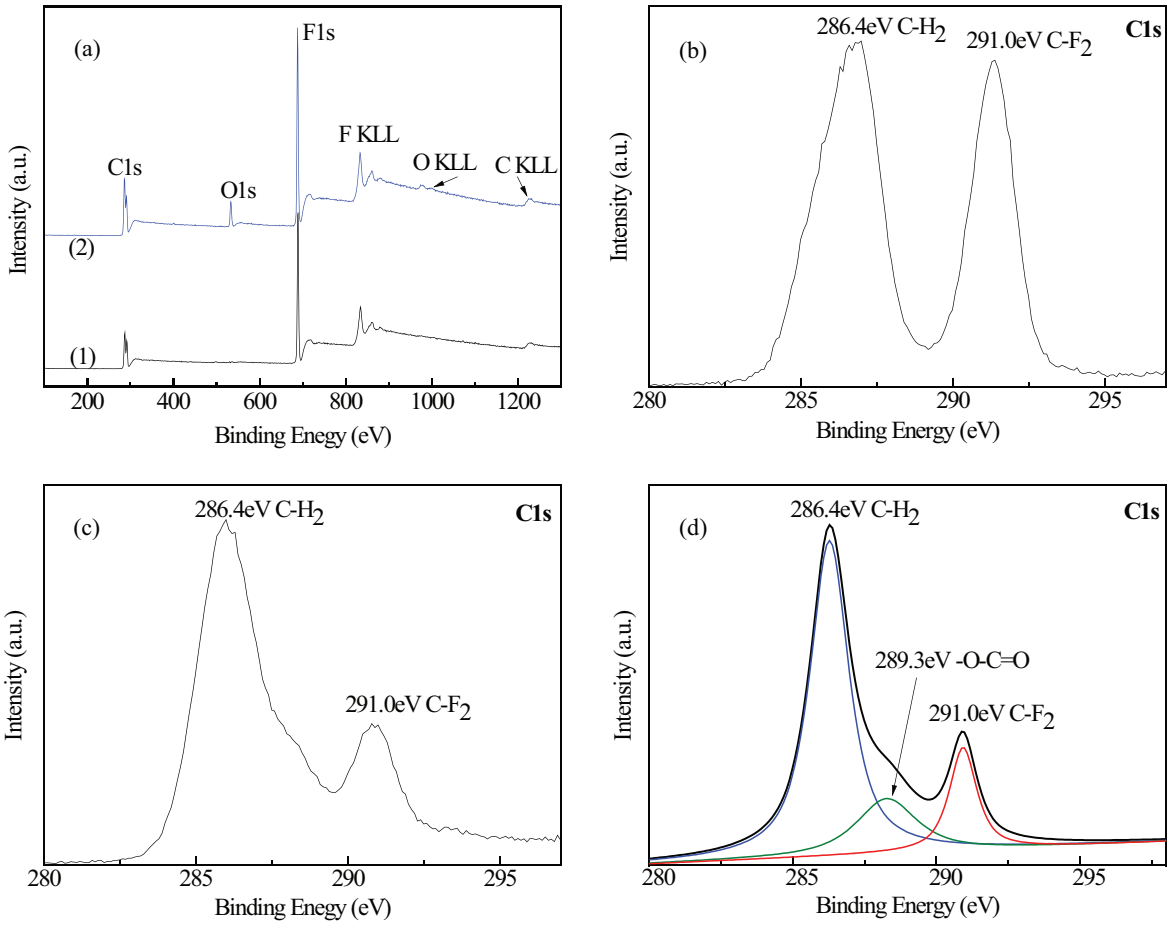

Fig. 7. XPS spectra of (a) the survey spectra of PVDF membrane and Cu(II)/MIM/PVDF, (b) C 1s spectra of PVDF membrane, (c) C 1s spectra of Cu(II)/MIM/PVDF, (d) C 1s spectra of Cu(II)/MIM/PVDF after fitting.

weight loss of the PVDF membrane takes place in the temperature range 455°C–610°C, and that the PVDF weightlessness ratio has two stages with different speed rates of 58.3% and 41.2%. In addition, the corresponding DTA curve has an obvious endothermic peak from membrane decomposition at 590.5°C. The decomposition ratio of the PVDF membrane can reach 99.46% at 610°C. In Fig. 8(b), the TGA curves show that the Cu(II)/MIM/PVDF begins to decompose at approximately 200°C, much higher than the operating temperature of membrane separation (20°C–30°C). Furthermore, it slowly appears to exhibit weightlessness in the temperature range 200°C–450°C. This may be the degradation of α-methacrylic acid and EDMA on the PVDF membrane surface. The weightless speed has two stages, with weightless ratios of 62.3% and 35.2%, caused by the fast fracture of the main chain. In the corresponding DTA curve, there are two obvious endothermic peaks form membrane decomposition, at 510°C and 611°C. The decomposition ratio of Cu(II)/MIM/PVDF can reach 98.76% at 635°C. The modified membrane layer shows significantly lower thermal stability than the PVDF membrane, indicating that the surface modification of the PVDF membranes affect the thermal stability of the PVDF membrane, but it still retains the advantage of good thermal stability of the unmodified PVDF membrane.

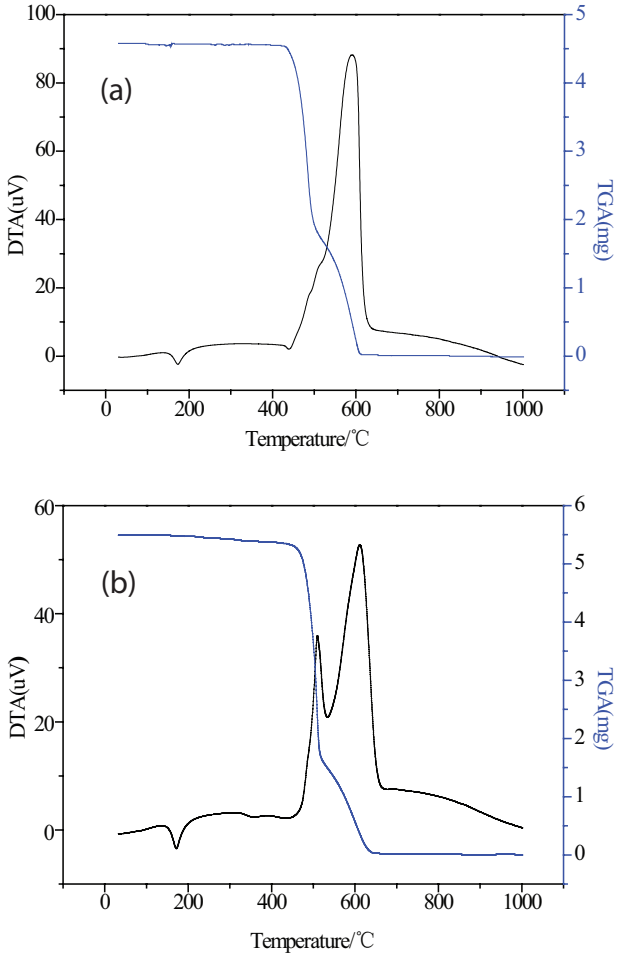

Fig. 8. The DTA–TGA data of (a) PVDF membrane and (b) Cu(II)/MIM/PVDF.

3.6. Hydrophobicity analysis of Cu(II)/MIM/PVDF

The CA and surface free energy of the membranes are shown in Fig. 9 and Table 1. It can be seen from the figure that the CA values decrease with a reduction in the ratio of the template molecule to the monomer, indicating an improvement of surface hydrophilicity of Cu(II)/MIM/PVDF, which can be interpreted by the process of molecularly imprinted modification on the membrane surface introducing hydrophilic groups of –COOH. With an increase in MAA content, which means more –COOH groups grafted onto the membrane surface, the hydrophilicity is gradually enhanced. The data in Table 1 show that the surface energy of the PVDF membrane is 24.95 mJ·m^{-2}, close to the value 25 mJ·m^{-2} reported in previous research [37]. Nevertheless, Cu(II)/MIM/PVDF with different ratios of the template molecule to the monomer of 1:4, 1:5, and 1:6 shows various surface energy data, 35.89, 39.5,

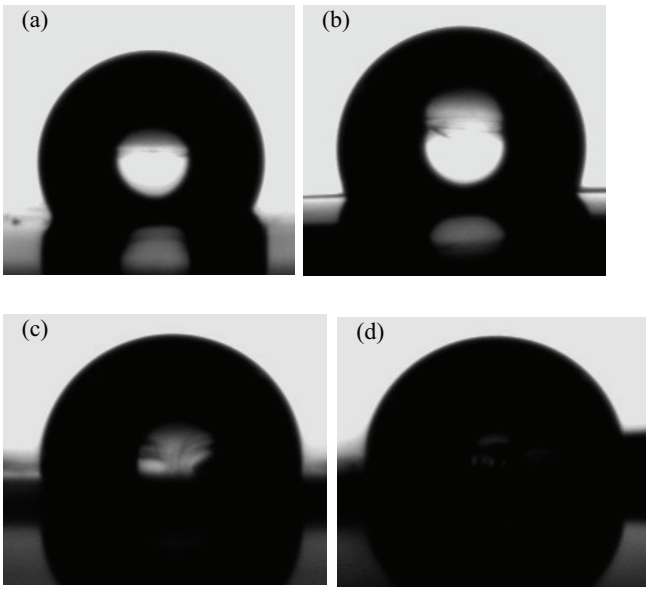

Fig. 9. The CA images of PVDF membrane and Cu(II)/MIM/PVDF with various ratio of template molecule and monomer (a) PVDF membrane, (b) 1:4 MIM/PVDF, (c) 1:5 MIM/PVDF, and (d) 1:6 MIM/PVDF.

Table 1
The surface energy and CA values of PVDF and Cu(II)/MIM/PVDF with various ratio of template molecule and monomer

Membrane type	PVDF	1:4 MIM/PVDF	1:5 MIM/PVDF	1:6 MIM/PVDF
Contact angle (°)	120	110.9	100.5	97.2
Surface energy (mJ·m^{-2})	24.95	35.89	39.5	40.49

and 40.49 mJ·m^{-2}, respectively, which are lower than that of water (72.8 mJ·m^{-2}), indicating that Cu(II)/MIM/PVDF possesses enough hydrophobicity applicable to the metal separation in water solution. Since excessive high hydrophilicity can improve the water flux, the membrane solvent may be easily lost under pressure, although higher hydrophilicity may make the combination of Cu(II) and microvoids easier to occur during the transfer process. Thus, it is necessary for Cu(II)/MIM/PVDF to possess a certain degree of hydrophobicity in the process of metal separation in water.

3.7. Mechanical property analysis

Stress–strain tests results are presented in Fig. 10, which shows that the influence of pre-treatments and surface modification on the mechanical properties of the membrane is very significant. After surface modification, the tensile strength of Cu(II)/MIM/PVDF decreases from 15.93 to 13.22 MPa. In addition, the strain at breaking of Cu(II)/MIM/PVDF significantly decreases from 39.00% to 34.04%. This implies that the elastic property or flexibility is weaker after surface modification. It is believed that the reduction in the membrane's mechanical strength after surface modification could be due to the degradation of polymer as a result of the dehydrofluorination occurring in the polymer chain [38].

3.8. Pure water flux of membrane

The pure water flux curves of the PVDF membrane and Cu(II)/MIM/PVDF are shown in Fig. 11. It can be seen from the figure that the pure water flux of the membrane is sharply reduced within 30 min, with base remaining unchanged after 90 min. Compared with the PVDF membrane, the pure water flux of Cu(II)/MIM/PVDF decreases slowly. The pure water fluxes of the PVDF membrane and Cu(II)/MIM/PVDF with ratios of the template molecule to the monomer of 1:4, 1:5, and 1:6 were calculated using Eq. (2) and are 200.0, 348.5, 361.8, and 344 L/(m^2·h), respectively. The pure water flux of Cu(II)/MIM/PVDF was remarkably improved. The pure water flux of Cu(II)/MIM/PVDF at different ratios of the template molecule to the monomer were different, but the change was small. This is because the hydrophilicity of the PVDF membrane has been enhanced through modification.

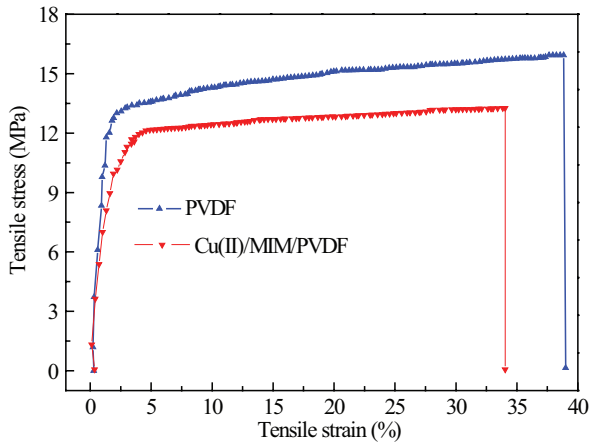

Fig. 10. Stress–strain plots of the membrane.

The membrane penetration resistance was also reduced, so that pure water flux was improved. At the same time, the membrane surface stain resistance has been enhanced.

Fig. 12 shows the rejection equilibrium curve of metal ions in the solution. It can be seen from Fig. 12(a) that the concentration of metal ions in the penetrating solution are higher than 1.5 × 10^{-4} mol L^{-1}, and that the rejection rates of Cu(II), Ni(II), Co(II), and Mn(II) are 61.8%, 61.2%, 61.5%, and 61.8%,

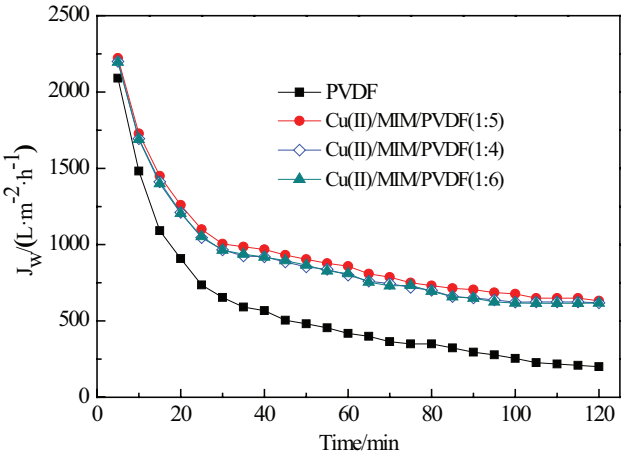

Fig. 11. The pure water flux curve of PVDF membrane and Cu(II)/MIM/PVDF.

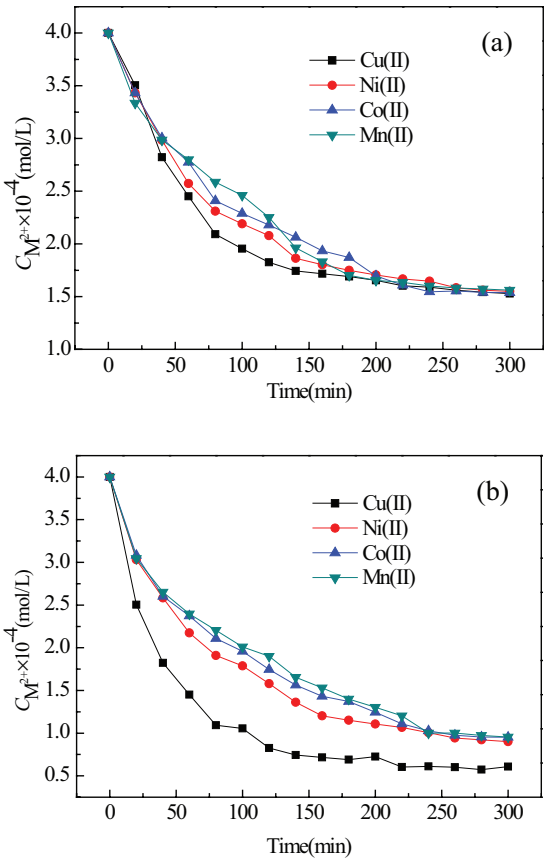

Fig. 12. The rejection equilibrium curve of metal ions (a) PVDF membrane and (b) Cu(II)/MIM/PVDF.

respectively. The metal ions rejection of the PVDF membrane made no obvious difference. Fig. 12(b) shows that the rejection rates of Cu(II), Ni(II), Co(II), and Mn(II) increase and are 84.8%, 77.5%, 76.2%, and 76.1%, respectively, of which the Cu(II) rejection rate has significantly increase after surface modification. This indicates that the prepared Cu(II)/MIM/PVDF for Cu(II) have a good rejection rate, and they can be used to separate and concentrate metal ions.

3.9. Selectivity analysis of Cu(II)/MIM/PVDF

A series of transfer experiments were performed through the PVDF membrane and Cu(II)/MIM/PVDF, and the results are plotted in Fig. 13. As shown in Fig. 13(a), the concentrations of four metal ions in the stripping solution increase gradually with an increase in transfer time. However, the rate of increase is disparate, which can be explained by the different complexation of carriers with various metal ions to form coordination compounds. On the other hand, the transfer rate of Cu(II) in Figs. 13(b)–(d) remains high, while the transfer rate of three other metal ions decreases obviously. This indicates that there is excellent selectivity of Cu(II)/MIM/PVDF for Cu(II), whereas Mn(II), Co(II), and Ni(II) cannot pass through the membrane due to the disaccordance with the shape of molecularly imprinted microvoids. At the same time, it can be seen from Figs. 13(b)–(d) that the effects on the metal ions selectivity of the three modified membranes are not obvious change. Moreover, the permeability coefficient of Cu(II) in Cu(II)/MIM/PVDF can reach 92%, showing a good transfer effect.

3.10. Permeability analysis of Cu(II)/MIM/PVDF

The transfer process is shown in Fig. 14 using $-\ln c_t/c_0$ and t. P_c can be taken as the slope of the dynamics curve. The slope of the PVDF-supported liquid membrane was calculated as 1.625 from the data in Fig. 14, while the slope of Cu(II)/MIM/PVDF-supported liquid membrane with different ratios of the template molecule and monomer of 1:4, 1:5, and 1:6 were 2.33, 2.47, and 2.11, respectively. The permeability of Cu(II)/MIM/PVDF with a ratio of the template molecule to the monomer of 1:5 was higher, indicating that the permeability of Cu(II)/MIM/PVDF for Cu(II) is higher than that of the PVDF membrane. This is mainly due to the strong hydrophobicity of the PVDF membrane surface, which can lead to a separation between the water phase and organic phase to impede the Cu(II) transfer. Although the pore diameter tends to be smaller after molecular imprinting, an increase in hydrophilicity leads to easy contact with the interface of the two phases, so that more Cu(II) can reach the interface to combine with the carrier and pass through the membrane.

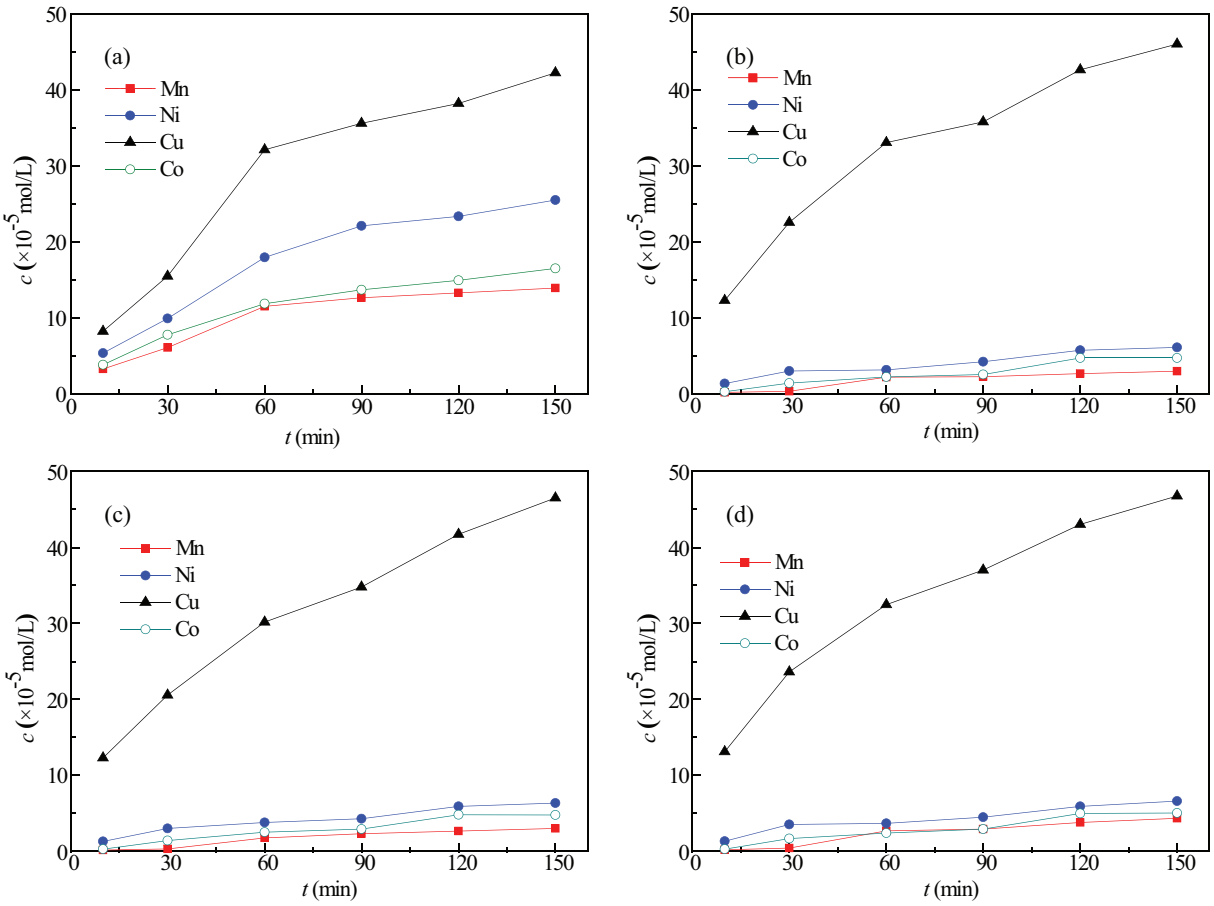

Fig. 13. The kinetic curves of concentration and time for various metal ions (a) PVDF membrane, (b) Cu(II)/MIM/PVDF (1:5), (c) Cu(II)/MIM/PVDF (1:4), and (d) Cu(II)/MIM/PVDF (1:6).

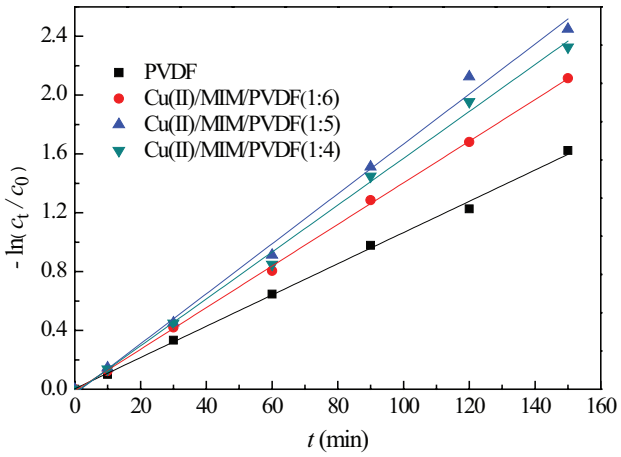

Fig. 14. Comparison of permeability coefficient between PVDF membrane and Cu(II)/MIM/PVDF.

4. Conclusion

The preparation and structural properties of Cu(II)/MIM/PVDF were investigated. The results clearly indicate that the microvoids of Cu(II)/MIM/PVDF are smaller than those of the PVDF membrane, and that they are distributed more evenly on the Cu(II)/MIM/PVDF surface. The MIM layer and PVDF membrane are combined through chemical bonds in the form of C–O bonds. The modified membrane can retain a good crystalline state and the thermal stability of the PVDF membrane. Moreover, the CA values of modified membrane decrease to 97°, while surface energy increases to 40.49 mJ m^{-2} by introducing a –COOH hydrophilic group, indicating an obvious increase in the hydrophilicity of the modified membrane. The pure water flux of modified membrane (361.8 L $(m^2 \cdot h)^{-1}$) is higher than that of the PVDF membrane (200.0 L $(m^2 \cdot h)^{-1}$). During the transfer process, Cu(II)/MIM/PVDF shows better selectivity and permeability for Cu(II) compared with the PVDF membrane. In summary, the feasibility of Cu(II)/MIM/PVDF is demonstrated by the above results. Thus, it is desirable to use molecular imprinting technology for metal ions removal in wastewater treatment in the future.

Acknowledgments

This work was supported by the National Science Foundation of China (Grant Nos. 21276208, 21576220), the S&T plan project of Shaan Xi Provincial Government (Grant No. 2015JZ005).

References

[1] X. Tang, H.L. Zheng, H.K. Teng, Y.J. Sun, J.S. Guo, W.Y. Xie, Q.Q. Yang, W. Chen, Chemical coagulation process for the removal of heavy metals from water: a review, Desal. Wat. Treat., 57 (2016) 1733–1748.

[2] R.R. Pawar, Lalhmunsiama, H.C. Bajaj, S.M. Lee, Activated bentonite as a low-cost adsorbent for the removal of Cu(II) and Pb(II) from aqueous solutions: batch and column studies, J. Ind. Eng. Chem., 34 (2016) 213–223.

[3] Y.H. Tang, Y.K. Lin, B. Zhou, X.L. Wang, PVDF membranes prepared via thermally induced (liquid-liquid) phase separation and their application in municipal sewage and industry wastewater for water recycling, Desal. Wat. Treat., 57 (2016) 22258–22276.

[4] H. Lee, E. Shim, H.S. Yun, Y.T. Park, D. Kim, M.K. Ji, C.K. Kim, W.S. Shin, J. Choi, Biosorption of Cu(II) by immobilized microalgae using silica: kinetic, equilibrium, and thermodynamic study, Environ. Sci. Pollut. Res., 23 (2016) 1025–1034.

[5] Y.J. Sun, H.L. Zheng, Z.P. Xiong, Y.L. Wang, X.M. Tang, W. Chen, Y. Ding, Algae removal from raw water by flocculation and the fractal characteristics of flocs, Desal. Wat. Treat., 56 (2015) 894–904.

[6] K. Wongkaew, T. Wannachod, V. Mohdee, U. Pancharoen, A. Arpornwichanop, A.W. Lothongkum, Mass transfer resistance and response surface methodology for separation of platinum (IV) across hollow fiber supported liquid membrane, J. Ind. Eng. Chem., 42 (2016) 23–35.

[7] B. Swain, C. Mishra, J. Jeong, J.C. Lee, H.S. Hong, B.D. Pandey, Separation of Co(II) and Li(I) with Cyanex 272 using hollow fiber supported liquid membrane: a comparison with flat sheet supported liquid membrane and dispersive solvent extraction process, Chem. Eng. J., 271 (2015) 61–70.

[8] M.H. Zhu, Y.B. Yun, W.Y. Xiang, Purification of *Ginkgo biloba* flavonoids by UF membrane technology, Desal. Wat. Treat., 51 (2013) 3847–3853.

[9] W.Z. Qiu, H.C. Yang, L.S. Wan, Z.K. Xu, Co-deposition of catechol/polyethyleneimine on porous membranes for efficient decolorization of dye water, J. Mater. Chem. A, 3 (2015) 14438–14444.

[10] S. Devi, P. Ray, K. Singh, P.S. Singh, Preparation and characterization of highly micro-porous PVDF membranes for desalination of saline water through vacuum membrane distillation, Desalination, 346 (2014) 9–18.

[11] M.F. Rabuni, N.M. Nik Sulaiman, N. Awanis Hashim, A systematic assessment method for the investigation of the PVDF membrane stability, Desal. Wat. Treat., 57 (2016) 1–12.

[12] H.P. Xu, W.Z. Lang, X. Zhang, Y.J. Guo, Preparation and characterizations of charged PVDF membranes via composite thermally induced phase separation (C-TIPS) method, J. Ind. Eng. Chem., 21 (2015) 1005–1013.

[13] S. Dai, Y. Seol, S. Wickramanayake, D. Hopkinson, Characterization of hollow fiber supported ionic liquid membranes using microfocus X-ray computed tomography, J. Membr. Sci., 492 (2015) 497–504.

[14] W.X. Zhang, L.H. Ding, J.Q. Luo, M.Y. Jaffrin, B. Tang, Membrane fouling in photocatalytic membrane reactors (PMRs) for water and wastewater treatment: a critical review, Chem. Eng. J., 302 (2016) 446–458.

[15] S. Arefi-Oskoui, V. Vatanpour, A. Khataee. Development of a novel high-flux PVDF-based ultrafiltration membrane by embedding Mg-Al nanolayered double hydroxide, J. Ind. Eng. Chem., 41(2016) 23–32.

[16] F. Korminouri, M. Rahbari-Sisakht, D. Rana, T. Matsuura, A.F. Ismail, Study on the effect of air-gap length on properties and performance of surface modified PVDF hollow fiber membrane contactor for carbon dioxide absorption, Sep. Purif. Technol., 132 (2014) 601–609.

[17] S. Rajabzadeh, D. Ogawa, Y. Ohmukai, Z. Zhou, T. Ishigami, H. Matsuyama, Preparation of a PVDF hollow fiber blend membrane via thermally induced phase separation (TIPS) method using new synthesized zwitterionic copolymer, Desal. Wat. Treat., 54 (2015) 2911–2919.

[18] I. Kim, D.C. Choi, J. Lee, H.R. Chae, J.H. Jang, C.H. Lee, P.K. Park, Y.J. Won, Preparation and application of patterned hollow-fiber membranes to membrane bioreactor for wastewater treatment, J. Membr. Sci., 490 (2015) 190–196.

[19] V. Buscio, M. Crespi, C. Gutiérrez-Bouzán, Application of PVDF ultrafiltration membranes to treat and reuse textile wastewater, Desal. Wat. Treat., 57 (2016) 8090–8096.

[20] T. Yuan, J.Q. Meng, T.Y. Hao, Z.H. Wang, Y.F. Zhang, A scalable method toward superhydrophilic and underwater superoleophobic PVDF membranes for effective oil/water emulsion separation, ACS Appl. Mater. Interfaces, 7 (2015) 14896–14904.

[21] A. Rahimpour, S.S. Madaeni, S. Zereshki, Y. Mansourpanah, Preparation and characterization of modified nano-porous PVDF membrane with high antifouling property using UV photo-grafting, Appl. Surf. Sci., 255 (2009) 7455–7461.
[22] T. Sun, Y. F. Zhang, C-L. Chen, X.Z. Gong, J.Q. Meng, Synthesis of membrane adsorbers via surface initiated ATRP of 2-dimethylaminoethyl methacrylate from microporous PVDF membranes, Chin. J. Polym. Sci., 32 (2014) 880–891.
[23] S. Scorrano, L. Mergola, M.P. Di Bello, M.R. Lazzoi, G. Vasapollo, R. Del Sole, Molecularly imprinted composite membranes for selective detection of 2-deoxyadenosine in urine samples, Int. J. Mol. Sci., 16 (2015) 13746–13759.
[24] Q. Xia, Y.B. Yun, Q. Li, Z.J. Huang, Z.X. Liang, Preparation and characterization of monodisperse molecularly imprinted polymer microspheres by precipitation polymerization for kaempferol, Des. Monomers Polym., 20 (2016) 201–209.
[25] K.K. Tadi, R.V. Motghare, Potentiometric selective recognition of oxalic acid based on molecularly imprinted polymer, Int. J. Electrochem. Sci., 8 (2013) 3197–3211.
[26] H.L. Cheng, X.F. Zhu, S.X. Yang, Y.X. Wu, Q. Cao, Z.T. Ding, A pH-controllable imprinted composite membrane for selective separation of podophyllotoxin and its analog, J. Appl. Polym. Sci., 128 (2013) 363–370.
[27] T. Kamra, S. Chaudhary, C. Xu, L. Montelius, J. Schnadt, L. Ye, Covalent immobilization of molecularly imprinted polymer nanoparticles on a gold surface using carbodiimide coupling for chemical sensing, J. Colloid Interf. Sci., 461 (2016) 1–8.
[28] D.S. Kim, D.H. Kim, B.S. Lee, G.Y. Moon, H.K. Lee, N.S. Yong, J.W. Rhim, Effect of surface modifying macromolecules on the properties of poly(vinylidene fluoride) membranes, J. Ind. Eng. Chem., 15 (2009) 393–397.
[29] J.L. Cao, S.J. Zhou, W.J. Kong, M.H. Yang, L. Wang, S.H. Yang, Molecularly imprinted polymer-based solid phase clean-up for analysis of ochratoxin A in ginger and LC-MS/MS confirmation, Food Control, 33 (2013) 337–343.
[30] P. Ding, Z.Z. Li, S.F. Tang, N. Song, L.Y. Shi, Preparation of self-supporting molecularly imprinted films via transition layer construction and RAFT polymerization, and their use in HPLC, Microchim. Acta, 180 (2013) 599–605.
[31] M. Kaykhaii, M. Khajeh, S.H. Hashemi, Magnetic molecularly imprinted polymer nanoparticles for selective extraction of copper from aqueous solutions prior to its flame atomic absorption determination, J. Anal. Chem., 70 (2015) 1325–1329.
[32] Y.C. Wang, J. Peng, J.Q. Li, M.L. Zhai, PVDF based ion exchange membrane prepared by radiation grafting of ethyl styrenesulfonate and sequent hydrolysis, Radiat. Phys. Chem., 130 (2017) 252–258.
[33] G. Kang, H. Yu, Z. Liu, Y. Cao, Surface modification of a commercial thin film composite polyamide reverse osmosis membrane by carbodiimide-induced grafting with poly(ethylene glycol) derivatives, Desalination, 275 (2011) 252–259.
[34] G.L. Zhang, S.F. Lu, L. Zhang, Q. Meng, C. Shen, J.W. Zhang, Novel polysulfone hybrid ultrafiltration membrane prepared with TiO_2-g-HEMA and its antifouling characteristics, J. Membr. Sci., 436 (2013) 63–173.
[35] S. Singha, T. Jana, Effect of composition on the properties of PEM based on ploybenzimidazole and ploy(vinylidene fluoride) blends, Polymer, 55 (2014) 594–601.
[36] W.Z. Lang, Z. Xuan, J.P. Shen, H.P. Xu, Z.L. Xu, Y.J. Guo, The contrastive study of chemical treatment on the properties of PVDF/PFSA and PVDF/PVP ultrafiltration membranes, Desalination, 341 (2014) 72–82.
[37] S. Boributh, A. Chanachai, R. Jiraratananon, Modification of PVDF membrane by chitosan solution for reducing protein fouling, J. Membr. Sci., 342 (2009) 97–104.
[38] N. Awanis Hashim, Y. Liu, K. Li, Stability of PVDF hollow fibre membranes in sodium hydroxide aqueous solution, Chem. Eng. Sci., 66 (2011) 1565–1575.